

Supporting Information

Multi-dimensional analysis of single particles with sequential dual-nanopipette sensors

Rui-Xue Gao,^a Si-Yu Tian,^a Ying Chen,^a Yu-Ting Qi,^a Limin Xiang,^{ab} Wei-Hua Huang^{ac}
and Xin-Wei Zhang^{*a}

^a College of Chemistry and Molecular Sciences, Wuhan University, Wuhan 430072, P. R. China.

^b Taikang Center for Life and Medical Sciences, Wuhan University, Wuhan 430072, P. R. China.

^c Department of Hepatobiliary and Pancreatic Surgery, Zhongnan Hospital of Wuhan University, Wuhan 430071, P. R. China.

*Corresponding author: Xin-Wei Zhang

E-mail: xinweizhang@whu.edu.cn

Table of Contents

1. Experimental Section
 - 1.1 Materials and Reagents
 - 1.2 Instrumentation and Measurements
 - 1.3 Fabrication of Glass Nanopipettes
 - 1.4 Assembly of Sequential Dual-nanopipette Sensors
 - 1.5 Preparation of PEI-modified Nanopipettes
 - 1.6 Preparation of Antibody-functionalized Nanopipettes
 - 1.7 Modification of PS Particles with Different Proteins
 - 1.8 Ion Current Measurements and Analysis
2. Supplementary Figures
3. References

1. Experimental Section

1.1 Materials and Reagents

N-hydroxysuccinimide (NHS) and 1-ethyl-3-(3-dimethylaminopropyl) carbodiimide hydrochloride (EDC) were purchased from Sigma-Aldrich Corporation (St. Louis, USA). Polyethyleneimine (PEI, linear, M.W. 25000) was obtained from Beyotime Biotechnology Co., Ltd. (Shanghai, China). Bovine serum albumin (BSA) and Tween-20 were purchased from BioFroxx (Einhausen, Germany). Polystyrene particles with different radiuses and surface-functionalized groups were acquired from Shanghai Huizhi Biotechnology Co., Ltd. (Shanghai, China). FITC-labeled polystyrene particles (PS-FITC, 500 nm-radius) and silica particles (SiO₂ NPs) were purchased from Jiangsu Zhichuan Technology Co., Ltd. (Nantong, China). Carcinoembryonic antigen (CEA), α fetoprotein (AFP), anti-CEA, and anti-AFP antibodies were purchased from Sangon Biotech Co., Ltd. (Shanghai, China). FITC-labeled anti-CEA and APC-labeled anti-AFP antibodies were purchased from Abcam Company (Wuhan, China). Low binding microcentrifuge tubes were purchased from Guangzhou Jet Bio-Filtration Co., Ltd. (Guangzhou, China). All other chemicals with analytical grade were obtained from Sinopharm Chemical Reagent Co., Ltd. (Shanghai, China) and unless stated otherwise were used as received without further purification. Deionized (DI) water (resistivity ≥ 18 M Ω /cm, Millipore Inc., USA) was used for rinsing and preparing all aqueous solutions. All solutions in the experiment were filtered through a 0.22 μ m Millipore filter before use.

1.2 Instrumentation and Measurements

Scanning electron microscopy (SEM) images were taken by field-emission scanning electron microscopes (Zeiss Sigma and Tescan Clara). The FIB sculpture was performed by a focused ion beam scanning electron microscope (Tescan Solaris). Electrochemical measurements were conducted by a CHI 660e electrochemical workstation (CHI Instruments) with Ag/AgCl reference electrodes at room temperature. Bright-field and fluorescent images were taken by inverted fluorescent microscopes (AxioObserver Z1, Zeiss) and confocal microscope (Confocal Microscope LSM 900, Zeiss). DLS measurements of the particles were detected by a Zetasizer Nano ZS (Malvern). A microforge (World Precision Instruments, $\times 40$ objective) was used to observe nanopipettes and fabricate sequential dual-nanopipette sensors. Amperometric recordings were achieved with a patch clamp amplifier (EPC-10, HEKA Electronics) coupled with a micromanipulator (TransferMan 4r, Eppendorf). A microinjector (FemtoJet® 4i, Eppendorf) was used to apply pressure.

1.3 Fabrication of Glass Nanopipettes

Borosilicate nanopipettes used for all experiments were fabricated via heating and pulling borosilicate glass capillaries (i.d. 0.58 mm, o.d. 1.0 mm; i.d. 1.12 mm, o.d. 1.5 mm; world precision Instruments, USA). To

ensure cleanliness, the glass capillaries were first pretreated in freshly prepared piranha solutions (30% H₂O₂/98% H₂SO₄ = 1:3) for 2 h to remove organic contaminants on the surface. Next, the capillaries were immersed in a clean solution (30% H₂O₂/NH₄OH/H₂O = 1:1:5) to make silicon hydroxyl disintegrate completely. Then, the capillaries were rinsed thoroughly with deionized water and anhydrous ethanol in turn and vacuum dried overnight at 75 °C. The nanopipettes in this work were all prepared by using the pipette puller. The geometry of nanopipette was characterized by SEM. The I-V curves can also be used to estimate the radius based on Equation (1)^{1,2}:

$$r = \frac{1}{\pi\kappa R \tan \frac{\theta}{2}} + \frac{1}{4\kappa R} \quad (1)$$

where r is the orifice radius of glass nanopipette, κ is the conductivity of the electrolyte solution, R is the measured resistance of the nanopipette, and θ is the cone angle.

1.4 Assembly of Sequential Dual-nanopipette Sensors

First, the shoulder of nanopipette 1 was evenly spread with epoxy resin. Subsequently, nanopipette 1 was inserted into nanopipette 2 from the back precisely with 1 cm length of the tip left outside. Finally, the junction between the backend of nanopipette 1 and nanopipette 2 was fixed by epoxy resin. The sequential dual-nanopipette sensor prepared by the above process was dried at room temperature for 8 h to cure completely.

1.5 Preparation of PEI-functionalized Nanopipettes

The PEI-modified nanopipettes were fabricated by the following steps according to the previous study.³ At the beginning, 1 μ L polyethyleneimine aqueous solution (PEI, 0.5 mg/mL) was injected into the nanopipette using a microloader, and then the nanopipettes were placed in air for 30 min to let the PEI absorb on the inner wall of the nanopipette by electrostatic interaction. Later on, the nanopipettes were heated and dried in the oven at 120 °C for 5 h. Finally, PEI-modified nanopipettes with positive charge were obtained.

1.6 Preparation of Antibody-modified Nanopipettes

As the scheme of surface functionalization steps shown in Fig. S14. Briefly, the chemical modification can be complicated in four procedures. First, PEI-modified nanopipettes were prepared in the same method above. Then, the nanopipettes were reacted with 2.5% GA in DI water for 2 h to generate an aldehyde-activated surface with GA covalently linked to the amine groups. After carefully removing the excess GA solution, the PBS solution carrying anti-CEA or anti-AFP was backfilled into the nanopipettes. To achieve better performance, an optimized antibody concentration of 0.1 mg/mL was selected as shown in Figure S18. The nanopipettes were incubated for 4 h at room temperature, allowing the antibody to covalently link to the aldehyde groups. This was followed by a block with 1% BSA (w/v) in 1 \times PBS for 1 h to passivate unreacted

aldehyde groups against nonspecific bindings. Finally, antibody-functionalized nanopipettes were obtained.

1.7 Modification of PS Particles with Different Proteins

0.5 mg of carboxyl-modified PS particles (500 nm-radius) were dispersed in MES buffer, then 1 mg of EDC and 1 mg of Sulfo-NHS were added and incubated for 30 min. After centrifugal washing, 50 µg CEA or AFP was mixed with the deposit and incubated for 5 h at room temperature. Finally, the BSA blocking procedure was performed to block redundant sites.

1.8 Ion Current Measurements and Analysis

During ion current measurement, the prepared sensor was backfilled with a buffer solution containing nanoparticles and anchored in a holder, then its tip was immersed in the external solution. Ag/AgCl electrodes were inserted inside the sensor (working electrode) and external bath (reference electrode), respectively. The ion current traces were continuously recorded by EPC-10 with a sampling rate of 10 kHz, and Bessel filtered at 2.9 kHz by “Patch Master” software, with the whole detection system placed in a Faraday cage. The resistive pulse signals were extracted and analyzed using a custom-written MATLAB code.

The conversion from the blocking current ($\Delta I/I_0$) of resistive pulse to the size of nanoparticle was proceeded based on the algorithm reported by Prof. Henry S. White^{4,5}:

$$\Delta I/I_0 = kr^3 \quad (2)$$

where k is a proportionality constant relating $\Delta I/I_0$ to the nanoparticle radius (r) and is associated with the geometry of the pipettes. Hence, for different nanopipettes, the value of k is different and can be determined by defining the population mean as equal to the mean value measured by SEM. In our experiment, the value of k_1 (k of pore 1) and k_2 (k of pore 2) were determined using the 498 nm-radius PS NPs, $k_1 = 0.83\%/(498 \text{ nm})^3$ and $k_2 = 0.77\%/(498 \text{ nm})^3$ were then used to measure the radius of nanoparticles with different sizes based upon their blocking current.

The relative standard deviation (RSD) of the particle radius distribution is calculated by dividing the standard deviation (σ) with the distribution mean (\bar{r}):

$$\sigma = \sqrt{\frac{\sum_{i=1}^n (r_i - \bar{r})^2}{n}} \quad (3)$$

$$RSD = \frac{\sigma}{\bar{r}} \quad (4)$$

The histogram plotting, scatter plot generation and curve fitting were performed by Origin Pro 2024. To evaluate the accuracy of the functionalized-SDNS for particle discrimination, receiver operating characteristic (ROC) analysis and the area under the curve (AUC) calculation were performed using IBM SPSS Statistics 26.0.

2. Supplementary Figures

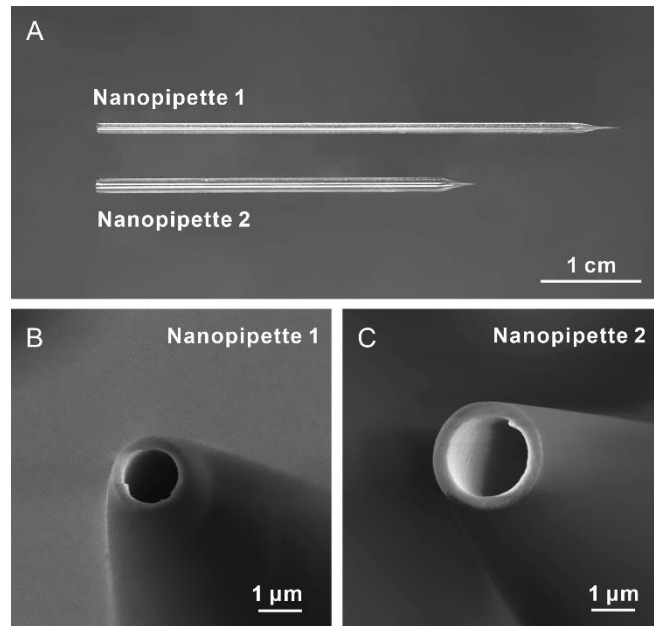


Figure S1. (A) Picture of the nanopipette 1 and nanopipette 2. Top-view SEM images of (B) nanopipette 1 and (C) nanopipette 2.

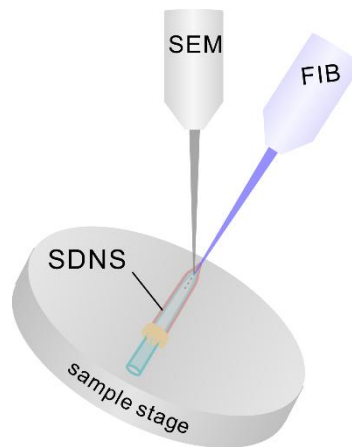


Figure S2. Illustration of FIB and SEM characterization system sculpt along the axis to expose profile inside of an SDNS.

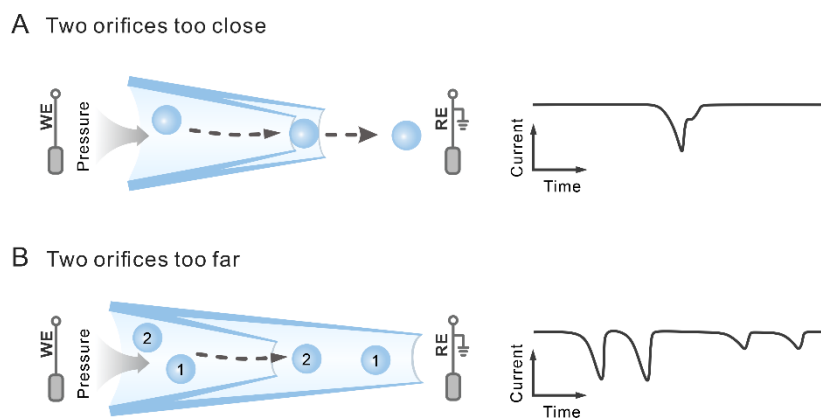


Figure S3. Schematic illustration of the SDNS in which the orifices of pore 1 and pore 2 are (A) too close or (B) too far and their corresponding typical spike signals.

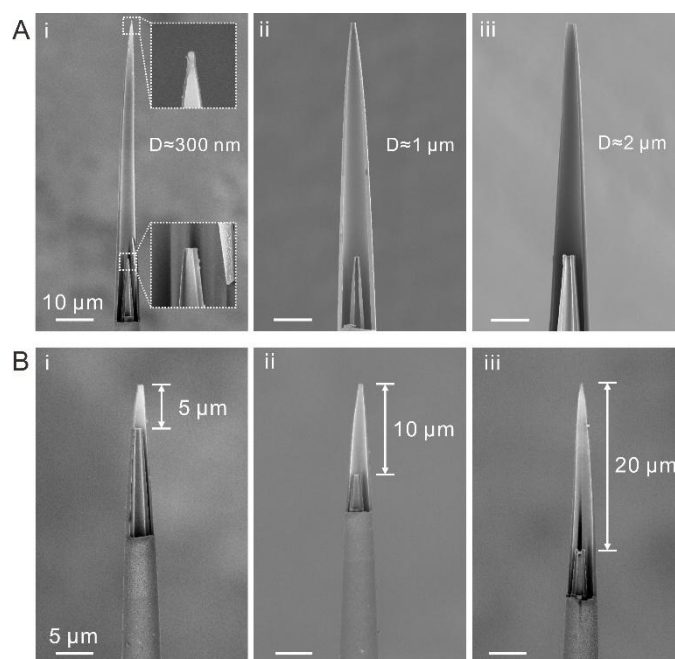


Figure S4. The SEM images of SDNS with (A) different apertures or (B) different distances between two pores.

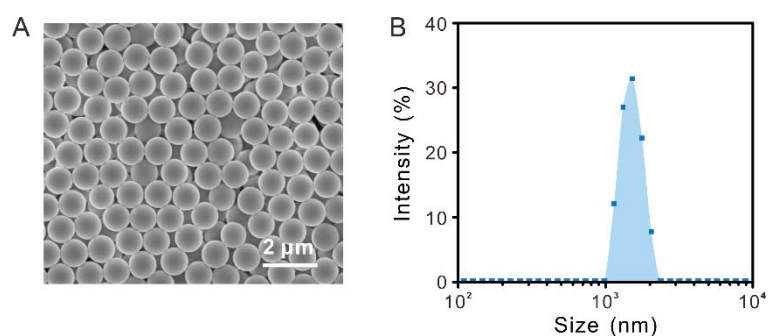


Figure S5. (A) SEM image of the 500 nm-radius PS NPs. (B) Dynamic light scattering (DLS) measured the size distribution (hydrodynamic diameter) of nominally 500 nm-radius PS NPs (20 $\mu\text{g/mL}$) in 10 mM PBST and the size distribution measured shows the presence of a homogenous suspension of nanoparticles.

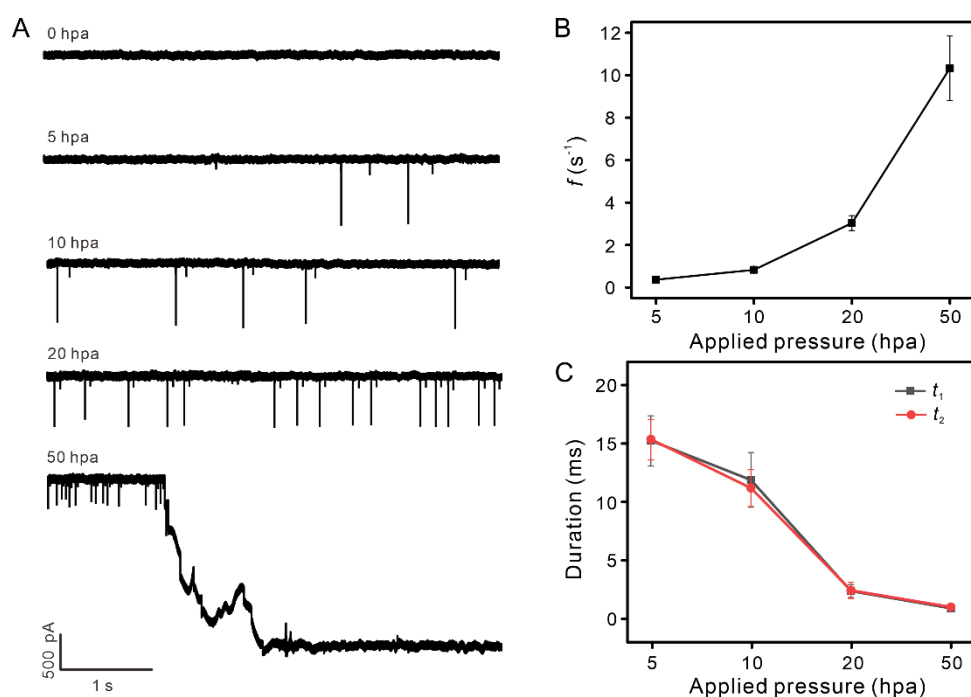


Figure S6. Optimization of applied pressure. (A) Current traces for the presence of 500 nm-radius PS NPs in 10 mM PBST at different pressures (internal vs external). (B) The change in the frequency of particle translocation (f) with respect to increasing pressures. (C) The change in the durations (t_1 and t_2) with increasing pressures. Error bars represent the standard deviation from three independent experiments.

In this experiment, different applied pressures (0, +5, +10, +20 and +50 hpa) were used to drive the particles. The results showed that the particle translocation frequency was increased with increasing the applied pressure, which contributed to the detection efficiency. However, the increase of the pressure also resulted in a decrease of the durations which was not conducive to the sufficient interaction between the particles and the surface of the nanopores. In addition, excessive pressure was also likely to cause permanent blockage of the pores. Therefore, a relatively small pressure (+10 hpa) was chosen to drive the particles to ensure that the particles can pass through the pores at a slow velocity while taking into account the signal frequency.

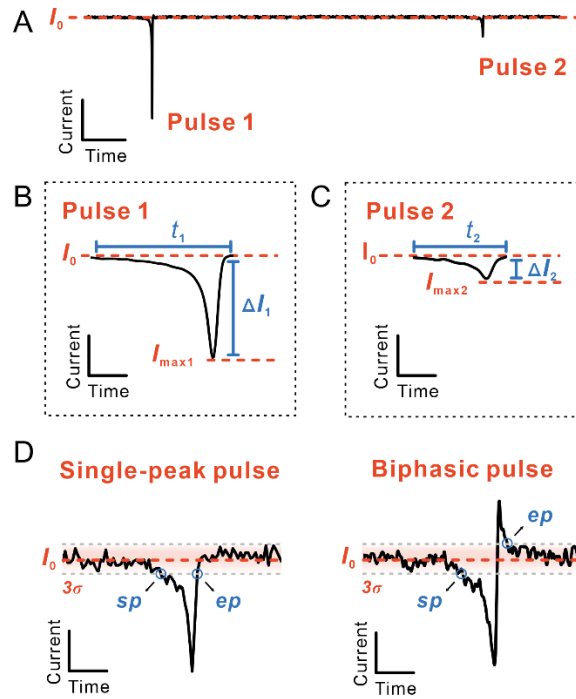


Figure S7. Definition of signal parameters. (A) A representative trace containing PS NP sensing events. The trace was acquired with SDNS as described in Figure 2. The enlarged view of (B) pulse 1 and (C) pulse 2. (D) Signal extraction schemes involve finding the baseline (I_0) and rms noise level (σ). An extraction threshold was set as 3-fold of the noise level, away from the local baseline. The starting point (sp) and ending point (ep) of the signals were extracted by finding points where the current trace crosses the thresholds ($I_0 \pm 3\sigma$). The interval between them was recorded as the duration (t) of the signal.

When a nanoparticle passes through the SDNS, two pulse signals would rise on the I - t curve. The signal (pulse 1) that appeared first came from the perturbation of the ionic current by the particle as it passed through pore 1. While the second pulse (pulse 2) was caused by the translocation of the particle through the pore 2. I_0 represents the open pore current of SDNS. I_{max1} and I_{max2} are the blockage currents, representing the peak current of pulse 1 and pulse 2, respectively. ΔI is defined as the absolute value of I_{max} minus I_0 ($\Delta I = |I_{max} - I_0|$), which stands for the height of the pulse. Furthermore, ΔI can be normalized by the nearby baseline and converted into the relative current amplitude ($\Delta I/I_0$). t stands for the duration, which is the full width of the pulse. To be specific, the duration is the interval between the starting point (sp) and ending point (ep) of the signals. For the single-peak I signals, the first data point lower than $(I_0 - 3\sigma)$ will be defined as the sp, while the first data point higher than $(I_0 + 3\sigma)$ will be defined as the ep. Whereas, for the biphasic pulses (as shown in Fig. 4C), the definition of the ep is a little different. The last data point higher than $(I_0 + 3\sigma)$ will be defined as their ep.

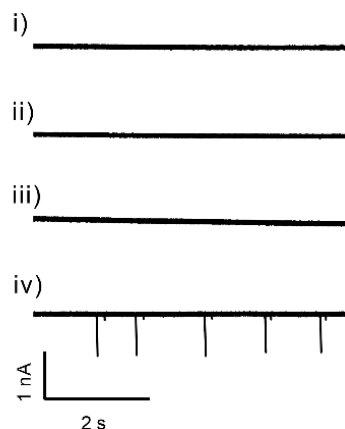


Figure S8. Current–time traces recorded with SDNS in 10 mM PBST. The sensor was biased at (i) -100 mV when no analyte was added and no pressure was applied; (ii) -100 mV when 500 nm-radius PS NPs were added inside the sensor but no pressure was applied; (iii) +100 mV when 500 nm-radius PS NPs were added inside the sensor but no pressure was applied; (iv) -100 mV when 500 nm-radius PS NPs were added inside the sensor with +10 hPa pressure was applied.

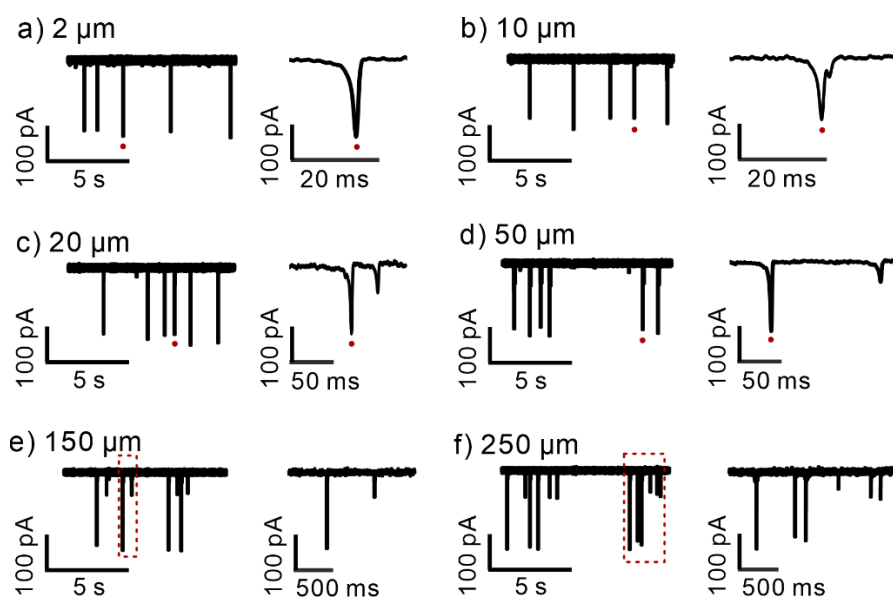


Figure S9. Current–time traces of 500 nm-radius PS NPs (dispersed in 10 mM PBST) recorded by the SDNS with different pore-to-pore distances and the enlarged view of the representative signals (pressure = +10 hpa).

In this experiment, a series of SDNS with different pore-to-pore distances were used to detect 500 nm-radius PS NPs. The results indicated that the SDNS with too short pore-to-pore distance would lead to complete or partial overlap between pulse 1 and pulse 2 (Figure S9a and S9b). As the distance extended to 20 μm , the pulses exactly separated from each other (Figure S9c). When SDNS with longer pore-to-pore distance was applied to detect the particles, the time interval between pulse 1 and pulse 2 could be further prolonged (Figure S9d and S9e). But the probability of different pulse pairs interlacing with each other would also increase accordingly. As shown in Figure S9f, there were multiple pairs of pulse signals interlaced together, making it difficult to match pulse 1 and pulse 2 of the same particle accurately. To effectively avoid the overlap

and interlacement between signals, the SDNS with pore-to-pore distance of around 20 μm was the proper choice. However, due to the different initial capillary diameters, SDNS with pore-to-pore distance below 50 μm and radius around 1-2 μm was relatively difficult to prepare. Therefore, taking into account the signal quality and the success rate of fabrication, SDNSs with pore-to-pore distance around 50 μm were mainly used in our work.

In view of the nanoparticle concentration is also a critical factor in confirming the single-particle resolution. Excessive particle concentrations will lead to the interlacing or even overlap of the signals from different particles. In order to avoid this problem, the upper limit of particle concentration was determined based on the experimental results. It was found that when the particle concentration was 1.14×10^8 particles/mL, the probability of signal overlap/interleaving was around 5% (pore-to-pore distance of the SDNS $\approx 50 \mu\text{m}$). Higher particle concentration will further increase this probability and cause the clogging of the pores. Therefore, to ensure the single particle resolution of the SDNS, the particle solution with concentration below of 1.14×10^8 particles/mL were used in our work.

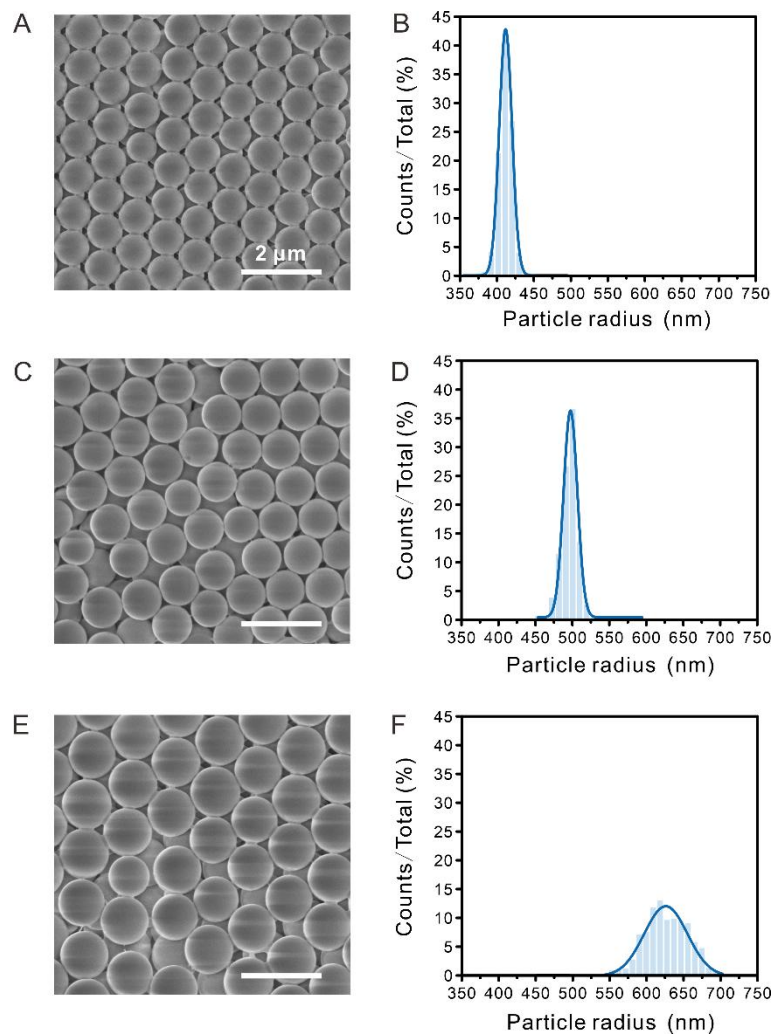


Figure S10. SEM images and the size distribution of nominally 400 nm (top panel), 500 nm (middle panel), and 600 nm (bottom panel) radius PS NPs.

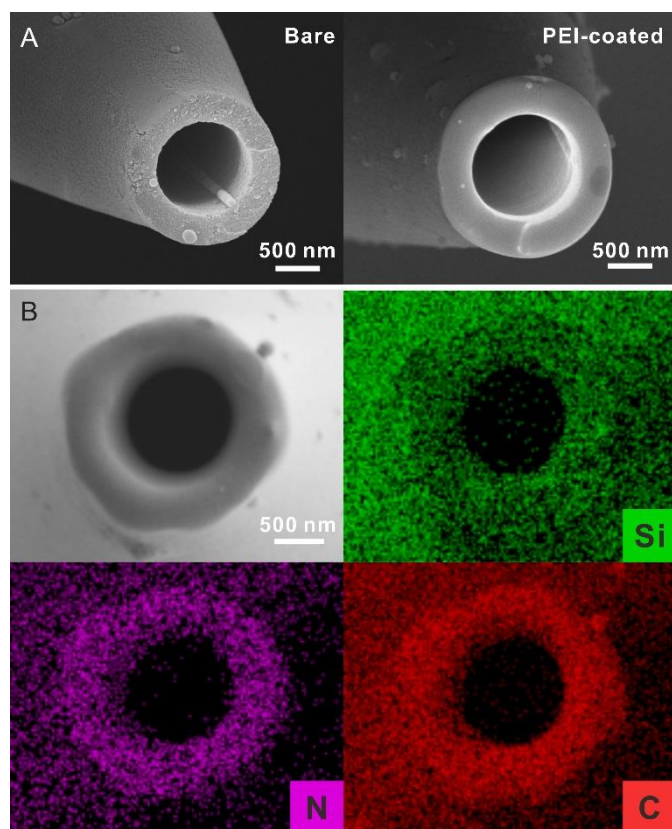


Figure S11. (A) SEM images of bare nanopipette and PEI-modified nanopipette. (B) SEM image of a PEI-modified nanopipette and its corresponding EDS elemental mapping images of Si (B, green), N (C, pink) and C (D, red).

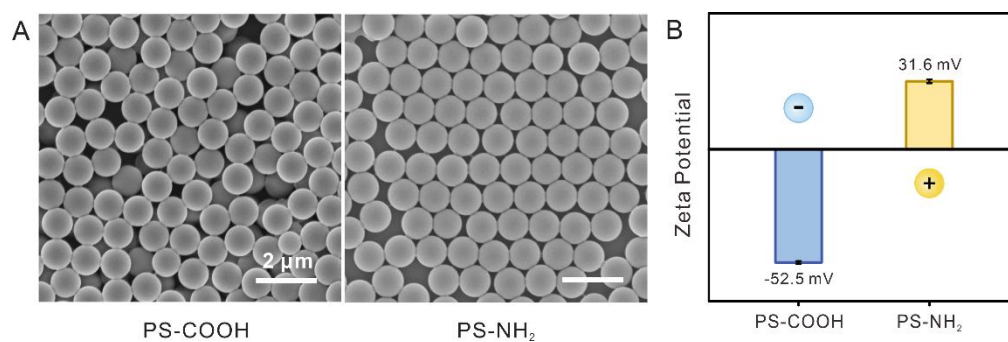


Figure S12. (A) SEM images of carboxy PS NPs (PS-COOH) and amino PS NPs (PS-NH₂) with 500 nm-radius. (B) The zeta potential of carboxy PS NPs (PS-COOH) and amino PS NPs (PS-NH₂) with 500 nm-radius in 0.5 mM PBST (pH = 7.0). The data were represented as mean \pm SD (n=3).

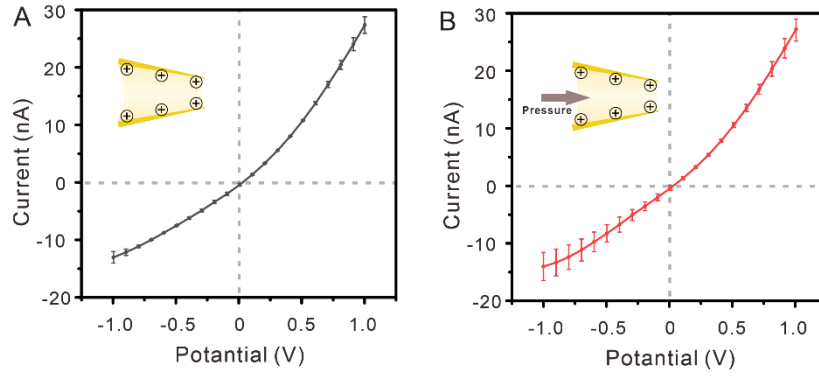


Figure S13. Current-voltage (I-V) curves of PEI-coated pore (A) in the absence of pressure and (B) with a +5 hPa pressure applied. The data were represented as mean \pm SD (n=3).

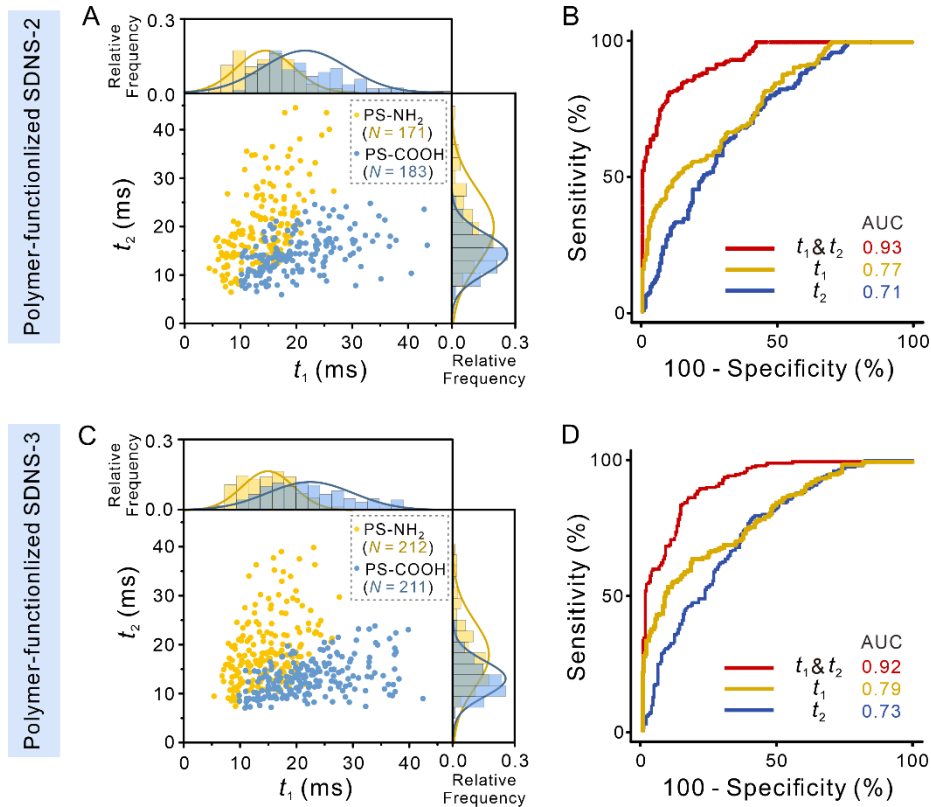


Figure S14. The duration distribution of two kinds of particles (PS-NH₂, yellow; PS-COOH, blue) translocating through pore 1 and pore 2 of polymer-functionalized (A) SDNS-2 and (C) SDNS-3. The corresponding ROC curves showing the performance of polymer-functionalized (B) SDNS-2 and (D) SDNS-3 for classifying PS-COOH and PS-NH₂ (pore 1, yellow line; pore 2, blue line; dual-pore, red line).

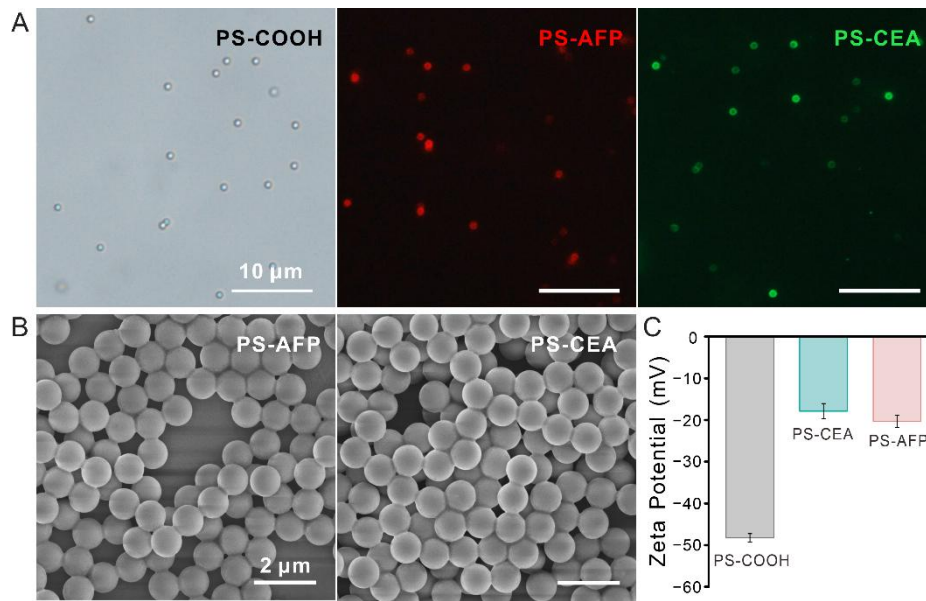


Figure S15. (A) Bright-field imaging of PS-COOH, fluorescence imaging of AFP-modified PS NPs and CEA-modified PS NPs. (B) SEM images of PS-AFP and PS-CEA. (C) The zeta potential of PS-COOH, PS-CEA and PS-AFP in 10 mM PBST (pH = 7.4). The data were represented as mean \pm SD (n=3).



Figure S16. The fabrication procedure of antibody-modified nanopipettes.

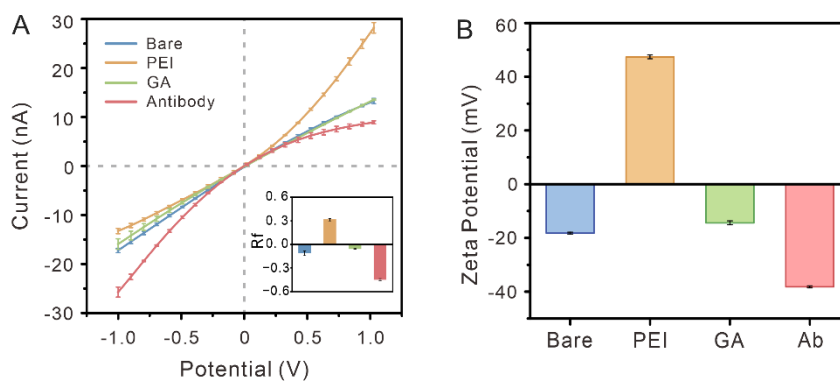


Figure S17. (A) Stepwise I-V responses of the antibody-modified nanopipette development. The supporting electrolyte was 10 mM KCl (pH 7.0). Inset: corresponding rectification factor. (B) The zeta potentials of Si NPs, PEI-Si NPs, GA-Si NPs and antibody-Si NPs, respectively. The data were represented as mean \pm SD (n=3).

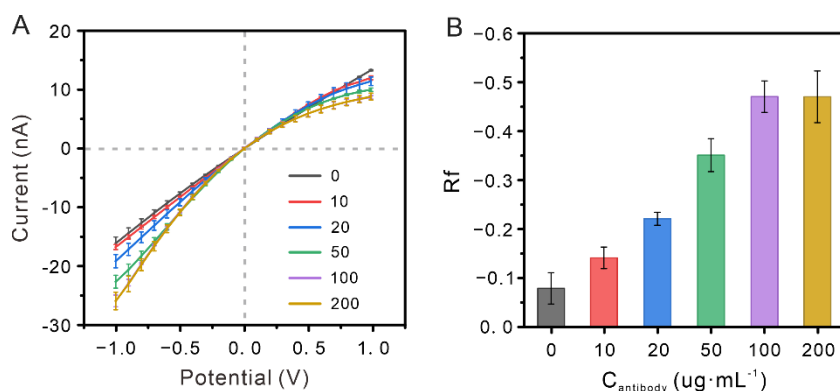


Figure S18. Optimization of antibody concentration. (A) Current-voltage (I-V) curves and (B) Rf of nanopipettes modified with antibody at different concentrations. The data were represented as mean \pm SD (n=3).

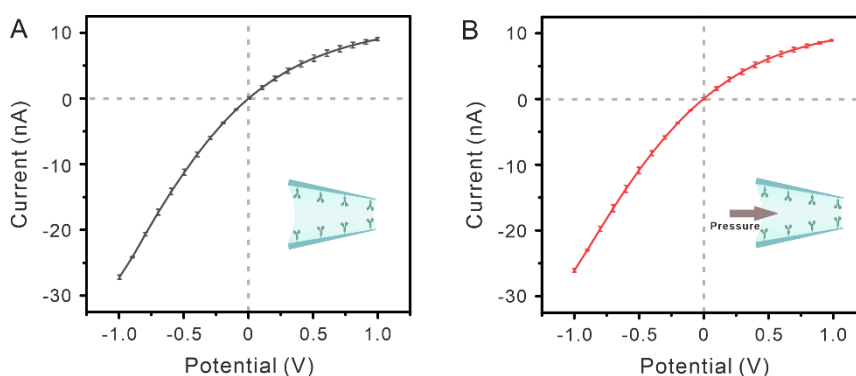


Figure S19. Current-voltage (I-V) curves of antibody-modified pores (A) in the absence of pressure and (B) with a +10 hPa pressure applied. The data were represented as mean \pm SD (n=3).

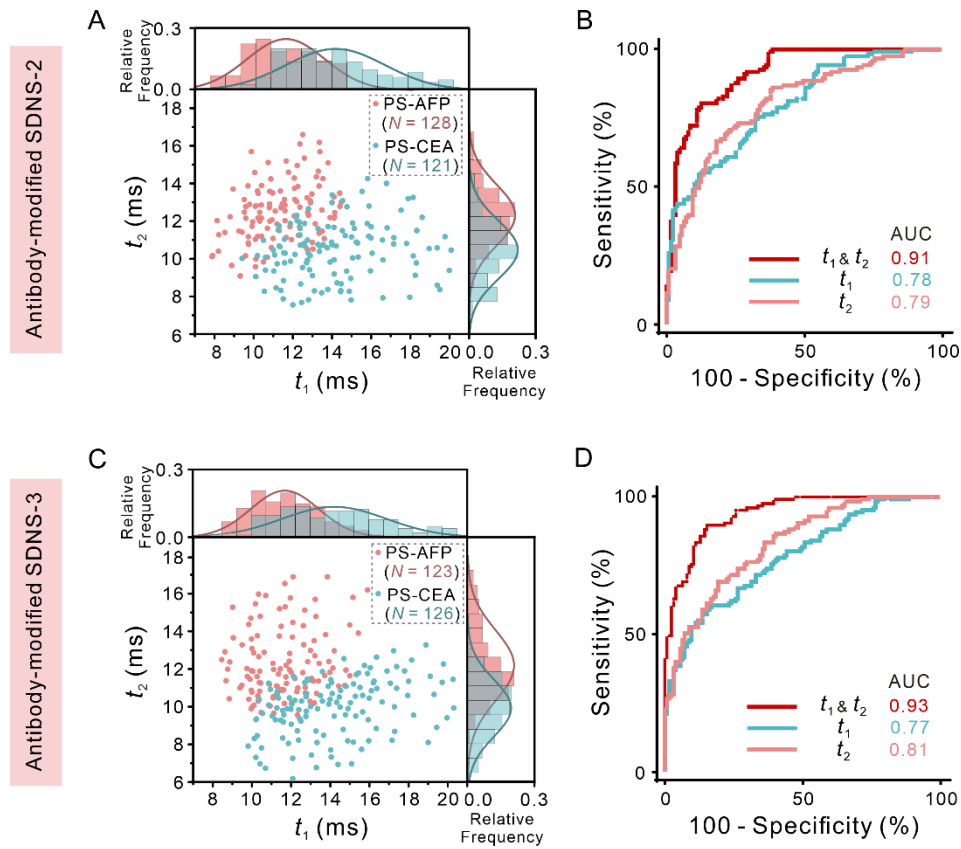


Figure S20. The duration distribution of two kinds of particles (PS-AFP, pink; PS-CEA, green) translocating through pore 1 and pore 2 of antibody-modified (A) SDNS-2 and (C) SDNS-3. The corresponding ROC curves showing the performance of antibody-modified (B) SDNS-2 and (D) SDNS-3 for classifying PS-AFP and PS-CEA (pore 1, green line; pore 2, pink line; dual-pore, red line).

3. References

1. D. Perry, D. Momotenko, R. A. Lazenby, M. Y. Kang, and P. R. Unwin, *Anal. Chem.* 2016, **88**, 5523-5530.
2. X. Y. Wang, T. M. Thomas, R. Ren, Yu Zhou, Peng ZhangJingjing LiShenglin CaiKai LiuAleksandar P. Ivanov*Andreas Herrmann*Joshua B. Edel*, *J. Am. Chem. Soc.* 2023, **145**, 6371-6382.
3. S. J. Liu, Y. T. Dong, W. B. Zhao, X. Xie, T. R. Ji, X. H. Yin, Y. Liu, Z. W. Liang, D. Momotenko, D. H. Liang, H. H. Girault, and Y. H. Shao, *Anal. Chem.* 2012, **84**, 5565-5573.
4. W. J. Lan, D. A. Holden, B. Zhang, and H. S. White, *Anal. Chem.* 2011, **83**, 3840-3847.
5. S. R. German, T. S. Hurd, H. S. White, and T. L. Mega, *ACS Nano* 2015, **9**, 7186-7194.